AFRL-OSR-VA-TR-2013-0114

CONTINUATION THROUGH SINGULARITY OF CONTINUUM MULTIPHASE ALGORITHMS

Xiaoyi Li, Marco Arienti

United Technologies Corporation

March 2013
Final Report

AIR FORCE RESEARCH LABORATORY
AF OFFICE OF SCIENTIFIC RESEARCH (AFOSR)
ARLINGTON, VIRGINIA 22203
AIR FORCE MATERIEL COMMAND

REPORT DOCUMENTATION PAGE

Form Approved
OMB No. 0704-0188

PLEASE DO NOT RETURN YOUR FORM TO THE ABOVE ADDRESS.

1. REPORT DATE *(DD-MM-YYYY)*	2. REPORT TYPE	3. DATES COVERED *(From - To)*
10-31-2012	Final Report	Aug 2009 - July 2012

4. TITLE AND SUBTITLE
CONTINUATION THROUGH SINGULARITY OF CONTINUUM MULTIPHASE ALGORITHMS

5a. CONTRACT NUMBER
FA9550-09-C-0191

5b. GRANT NUMBER

5c. PROGRAM ELEMENT NUMBER

6. AUTHOR(S)
Li, Xiaoyi
Arienti, Marco

5d. PROJECT NUMBER

5e. TASK NUMBER

5f. WORK UNIT NUMBER

7. PERFORMING ORGANIZATION NAME(S) AND ADDRESS(ES)
United Technologies Corporation
United Technologies Research Center
411 Silver Lane
East Hartford CT 06118-1127

8. PERFORMING ORGANIZATION REPORT NUMBER

9. SPONSORING/MONITORING AGENCY NAME(S) AND ADDRESS(ES)
Air Force Office of Scientific Research
875 N. Randolph St. Room 3112
Arlington VA 22203
Dr. Fariba Fahroo

10. SPONSOR/MONITOR'S ACRONYM(S)
AFOSR

11. SPONSOR/MONITOR'S REPORT NUMBER(S)
AFRL-OSR-VA-TR-2013-0114

12. DISTRIBUTION/AVAILABILITY STATEMENT
Distribution Statement A: Approved for public release; distribution is unlimited.

13. SUPPLEMENTARY NOTES

14. ABSTRACT
The mathematical singularities in continuum multiphase simulations were demonstrated by investigating a set of canonical problems of drop pinching off. The singularities were identified as arising from continuum Navier-Stokes formulation, indicating a physics-based closure model required to bypass the singularities. The study of detailed pinch-off physics was enabled by the development of a mesoscale approach based on particle-based formulation that bridges molecular and continuum scales. Simulation results using the mesoscale approach revealed the existence of a universal scaling law in quantifying the interface behaviors near pinch-off. A closure model for the continuum simulation was then developed based on the mesoscale scaling analysis. Physically/mathematically converged simulations of drop pinch-off were demonstrated using the continuum solver enhanced with the closure model.

15. SUBJECT TERMS

16. SECURITY CLASSIFICATION OF:			17. LIMITATION OF ABSTRACT	18. NUMBER OF PAGES	19a. NAME OF RESPONSIBLE PERSON
a. REPORT	b. ABSTRACT	c. THIS PAGE			Xiaoyi Li
UU	UU	UU	UU	33	19b. TELEPHONE NUMBER *(Include area code)* 860-610-7646

Reset

Standard Form 298 (Rev. 8/98)
Prescribed by ANSI Std. Z39.18

CONTINUATION THROUGH SINGULARITY OF CONTINUUM MULTIPHASE ALGORITHMS

CONTRACT FA9550-09-C-0191

FINAL REPORT

Xiaoyi Li
United Technologies Research Center,
MS 129-29,
411 Silver Lane,
East Hartford, CT 06118,
Tel. 860 610 7646, lixy2@utrc.utc.com

0.1 Objectives

The United Technologies Research Center (UTRC), a Division of UTC, was funded by AFOSR Computational Mathematics Program to investigate a class of singularities that arise in mathematical models describing interface dynamics in multiphase flow. The main focus was the process of liquid ligament pinch-off, the understanding of which is crucial to the first-principle modeling of fuel spray atomization. The singularities arise from the continuum Navier-Stokes formulation of two-phase flow as liquid-gas interfaces approach each other towards pinch-off. Physically, the continuum concept of surface tension at an infinitesimally thin interface does not hold when molecular fluctuations begin to be comparable to inertial and viscous forces. The question to be addressed is whether there is a unique continuation (through singularity) of the continuum solution obtained from the model discretization implemented in multiphase algorithms. From the computational standpoint, the crucial point is whether initial conditions after the singularity depend on the details of the numerical discretizations leading to pinch-off.

The objective of the project is to develop a physically/mathematically consistent multi-scale computational approach to continue the solution through the formal singularity described above. The multi-scale approach consists of a macroscopic, time-resolved interface-capturing simulation of two-phase flow; a singularity-free mesoscopic simulation that bridges atomic and continuum scales; and a physics-based closure model derived from the mesoscopic analyses to be embedded into the macroscopic continuum to bypass the singularity issue.

0.2 Summary of accomplishments

The overall objective of developing a mathematically/physically consistent multiscale and multiphase numerical approach to continue simulations through singularities due to topological changes of the interface was accomplished. The simulation framework developed under this project will be applied to future high-fidelity simulations of engine spray

atomization to accurately predict fuel droplet statistics and guide engine design, and it is expected to have a substantial impact in the jet-engine industry.

Towards the first objective of documenting and explaining the inconsistencies of continuum direct numerical simulations of non-disperse two-phase flow, it was successfully demonstrated that the mathematical singularity of assuming an infinitesimally thin interface near the pinch-off of a liquid jet leads to divergence of simulation in terms of interface position and flow pressure. An advanced interface-capturing multiphase solver developed previously by UTRC was used to simulate a canonical case of drop pinch-off under capillary and straining effects. After the lack of convergence with grid refinement was demonstrated, several algorithms were tested to bypass the pinch-off singularity by numerically forcing breakup at an assigned threshold. The results are documented in Subsection 1.1.

To achieve a better understanding of interface fluctuations, the project next was focused on developing a mesoscopic simulation approach that bridges molecular and continuum scales. The development was based on the general framework of dissipative particle dynamics (DPD). Several accomplishments are worth mentioning. A many-body dissipative particle dynamics (MDPD) code, obtained by combining short-range repulsive and long-range attractive forces, was applied to vapor/liquid simulations. Based on the radial distribution of the virial pressure in a drop at equilibrium, a systematic study was carried out to characterize the sensitivity of the surface tension coefficient with respect to the inter-particle interaction parameters: particularly, the approximately cubic dependence of the surface tension coefficient on the bulk density of the fluid was evidenced for the first time. In capillary flow, MDPD solutions were shown to satisfy the Plateau-Rayleigh condition on the wavelength of an axial disturbance leading to the pinch-off of a cylindrical liquid thread; correctly, no pinch-off occurred below the cutoff wavelength. The results are documented in subsection 1.2.

The objective of developing a coupling between the particle (P) and continuum (C) formulation was limited to the one-way coupling of the continuum simulation providing time-dependent boundary conditions to the particle simulation. This required the development of a Non-Periodic Boundary Condition (NPBC) algorithm for two-phase flow that can preserve a liquid gas interface through a non-periodic boundary. Several non-periodic algorithms are described in the literature for bulk flow fluid dynamics, but none, to the PIs' knowledge, for free surface flow. The full two-way coupling was found to be irrelevant to the overall objective of developing a closure model to allow continuation through singularity. Particularly, it was found that the objective of two-phase flow applications only require small-scale information to be fed into the large-scale simulation, and not vice-versa. Thus only one-way coupling is required. The funding was then focused on the development of a physics-based closure model and a generic implementation of the model in the continuum direct numerical simulation.

To develop a continuum closure model based on detailed physics, scaling analysis was performed on the mesoscopic simulation results from MDPD. The analysis illustrates the cascade of fluid dynamics behaviors from potential to inertial-viscous to stochastic flow, and the dynamics of a liquid jet minimum radius is consistent with the power law scaling predictions from asymptotic analysis. One major accomplishment is the key finding that the scaling transition is dependent on fluid properties only and independent of external flow conditions. The transition point can therefore be used as the threshold to enforce numerical breakup, leading to physically accurate and grid converged solutions. Because of the condition-independent nature of the threshold, the same threshold for breakup can be applied

for any pinch-off processes occurring in the simulation domain, independently from their local strain environment. Thus, the scaling transition point becomes the only parameter for the closure model. This model was implemented in the continuum two-phase flow solver in a completely grid-independent fashion. The implementation was demonstrated to converge under the physical breakup threshold and thus provide physically, mathematically and computationally consistent results. These results are documented in subsection 1.3 and 1.4.

0.3 Organization of the report

A comprehensive set of results is available in published papers and from the proceedings of conferences attended by the PI's. In this report, we provide more details for the key results obtained during the project. References to journal papers, conference papers and presentations are provided. A list of references is available in the last chapter of the report.

Contents

Chapter 1

Summary of research results

While multiphase flow involving complex topological changes occurs in a wide range of Air Force applications, observation of the multi-scale interfacial dynamics in a laboratory is limited by the difficulty in controlling the boundary conditions of the experiment and by constraints on instrument time response versus available field of view. The development of a mathematically correct and computationally feasible approach is a key step to achieve a deep understanding of the process.

This project aims to address a fundamental limitation in the first-principle simulations of multiphase flow. Asymptotic analysis indicates that the Navier-Stokes (NS) equations for multiphase flow lead to interface singularities. In this report, the limitation of simulations based on the discretization of multiphase NS equations is first demonstrated using a macroscopic Coupled Level Set and Volume Of Fluid (CLSVOF) interface-capturing approach (subsection 1.1). To identify when microscopic dynamics affects macroscopic physics, a computer code based on Many-body Dissipative Particle Dynamics (MDPD) was developed that bridges molecular and continuum scales (subsection 1.2). This effort enabled the creation of a "virtual test facility" for small-scale multiphase flow, whose results do not depend on prior calibration. The "facility" allows the derivation of detailed asymptotic results for pinch-off (subsection 1.3) and the development of a closure model embedded in the macroscopic simulation to achieve physically/mathematically consistent results in the presence of liquid pinch-off (subsection 1.4). The main elements of this research are summarized in the sketch below.

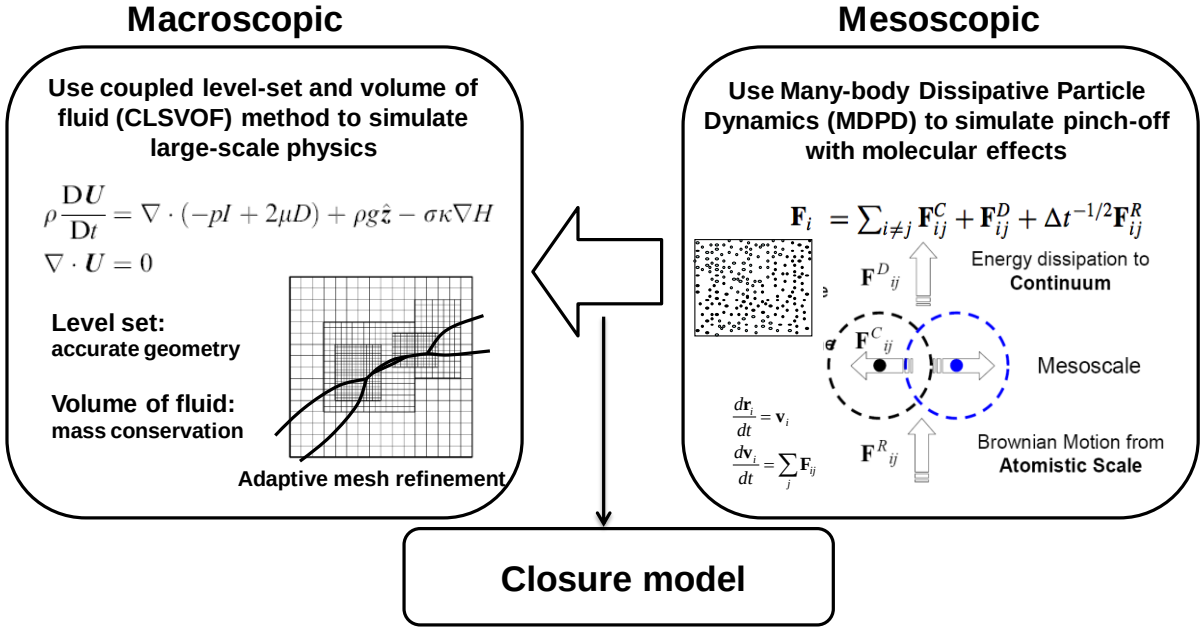

Figure 1. Summary of research elements for the investigation of computational continuation through multiphase singularity.

1.1 Demonstration of singularity in continuum two-phase simulations

1.1.1 Continuum two-phase approach

In the continuum approach adopted for this project, the CLSVOF method [1] is used to directly capture the evolution of a liquid-gas interface. Briefly, the Navier-Stokes equations for incompressible flow of two immiscible fluids are augmented with a smooth level set function ϕ, whose zero level represents the time-evolving interface. In addition to the evolution equation for ϕ, the transport equation for the cell liquid volume fraction (the volume-of-fluid function, F) is also solved. The interface normals used in the VOF reconstruction step are determined from the level set function. The volume fractions and the normals are then used to construct a volume preserving distance function ϕ. Essentially, volume is preserved by implementing a ''local'' mass correction at every iteration. Second-order accurate curvature is calculated from F by the method of height fraction.

The solver is implemented under the framework of adaptive mesh refinement (AMR) to reduce the computational cost of resolving multi-scale interface dynamics. A detailed description of the block-structured AMR can be found elsewhere [2]. Cells that are crossed by the liquid-gas interface are tagged for refinement. Starting from the base level, boxes (with a minimum size of, say, 32^3 cells) are combined to cover all the tagged cells within assigned coverage efficiency. This set of blocks with the same grid spacing forms level 1. This level is in turn tagged for refinement at the interface, and the process is repeated until the required grid resolution is achieved. The block-structured AMR framework allows easy implementation of special finite differencing schemes for multiphase flow on Cartesian grids.

1.1.2 Singularity demonstration in continuum simulations

We consider the pinch-off of a dumbbell-shaped drop due to either capillary effects or elongation effects in a straining flow. The simulation convergence is tested by a grid-refinement study using AMR. The lack of convergence in the simulations shown next points to the singularity due to the topology change of the drop. The axisymmetric water drop is immersed in an extensional flow, as shown in Fig. 2, with velocity field

$$u_r(r,x) = -\dot{\gamma} r / 2$$
$$u_x(r,x) = \dot{\gamma} x \quad ,$$

where $\dot{\gamma}$ is the straining rate. The center of the drop overlaps with the stagnation point of the extensional flow. Its initial shape is prescribed as

$$r(x) = \begin{cases} 0.5D - \varepsilon \cos(2\pi x / \lambda) & |x| < 0.5\lambda \\ \sqrt{(0.5D)^2 - (|x| - 0.5\lambda)^2} & 0.5\lambda \le |x| \le 0.5\lambda + 0.5D \end{cases} .$$

In the absence of the external straining flow, the drop may experience breakup driven by capillary effects or recover to spherical shape, depending on the ratio λ/D being larger or smaller than π [27]. With extensional straining, the drop can be elongated and finally broken

by the external flow if the strain rate is large enough. Here we select two different values of wavelength, under which the drop breaks up by capillary effects (λ/D=3.75>π) and by elongation at high strain rate λ/D=2.5<π, $\dot{\gamma} = 10^3\ s^{-1}$), respectively.

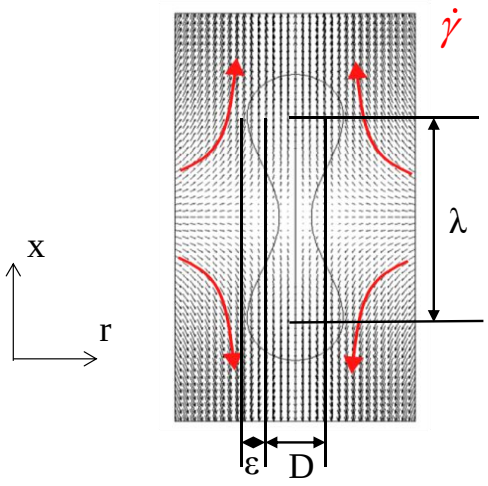

Figure 2. The dumbbell-shaped water drop placed in the center of an extensional straining air flow.

In the following tests, the computational domain is set to be 15 cm × 60 cm and covered with a uniform base grid of 64 × 256. Refinement was performed by successively adding refinement levels near the water-air interface, yielding effective grid resolutions of 128 × 512 at one level and 256 × 1024 at two levels.

The locations of the water-air interface prior to, near, and post pinch-off are shown in Fig. 3 for the capillary case ($\dot{\gamma} = 0$), in (a), and for the straining case ($\dot{\gamma} = 10^3\ s^{-1}$), in (b). Results from different refinement levels are shown together in the same plots. It can be observed that the interface locations converge prior to pinch-off for both cases. Near pinch-off, discrepancies between different refinement levels are observed, and even larger discrepancies are found post pinch-off. Comparing the two cases in (a) and (b), we find that the breakup under the straining flow is more sensitive to grid discretizations for this set of conditions. The interface disconnects due to numerical interface capturing issues when the neck region becomes under-resolved.

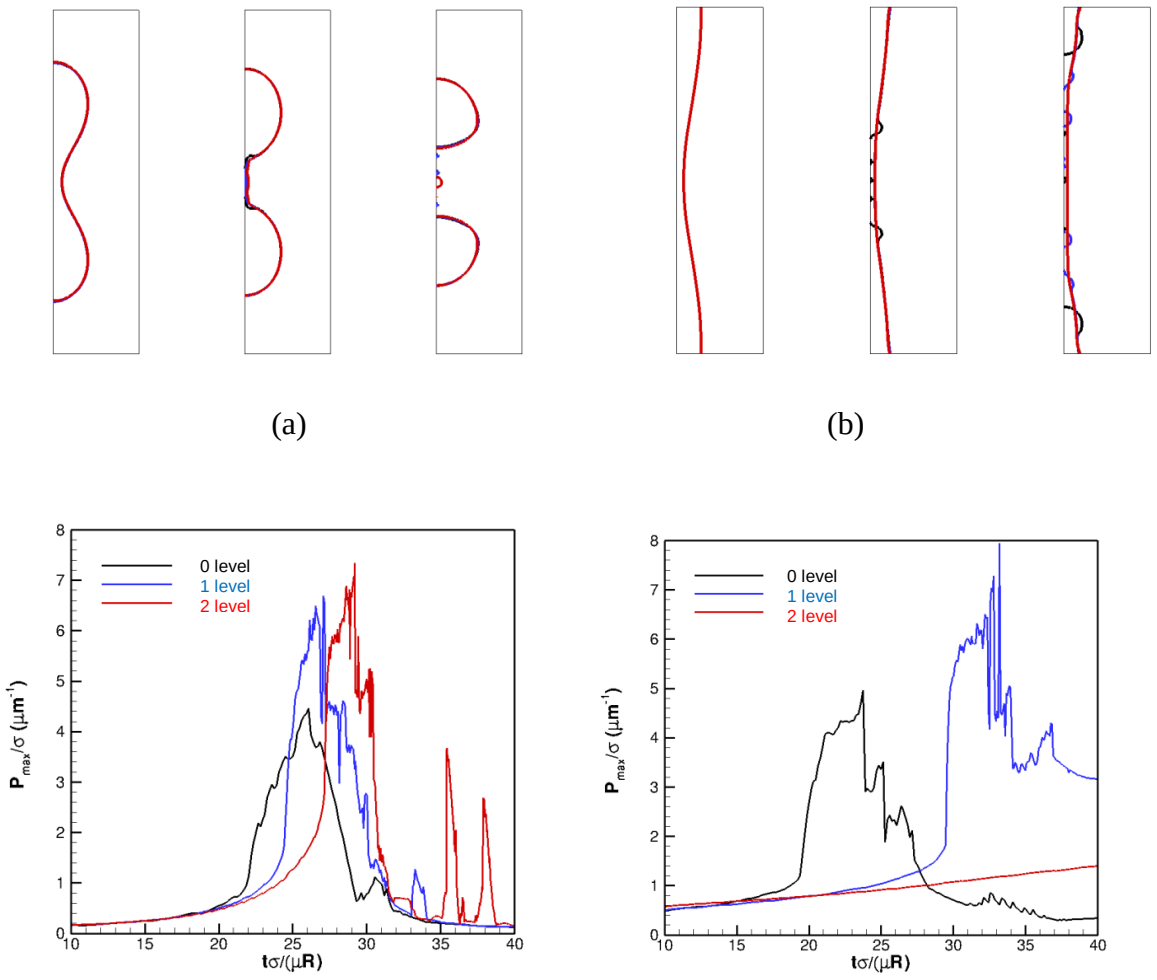

Figure 3. The interface location predicted using different resolutions for the capillary case (a) and extensional case (b). Corresponding maximum pressure at the pinch-off location for the capillary case in (c) and the extensional case in (d).

The corresponding maximum pressure at the pinch-off location is plotted in Fig. 3(c) for the capillary case and in Fig. 3(d) for the straining case. Both sets of curves show that the maximum local pressure, as a function of time reaches a peak at pinch-off. At different grid resolutions, the peak values differ, increasing with decreasing grid size because of smaller ligament width that can be resolved by the grid and therefore higher interface curvatures. It can be extrapolated that the pressure will not converge with further increase of resolution because the theoretical value of pressure approaches infinity at pinch-off. Because of the lack of convergence, the prediction of pinch-off time becomes highly sensitive to grid resolution. As shown in Fig.3 (c) and (d), the peak pressure shows up at different times for different grid resolutions and the discrepancies are further amplified in the extensional case (d) compared to the capillary case (c).

The above simulation results tell that a grid-converged simulation of pre-pinch-off liquid-gas interface diverges when the interface approaches pinch-off point. This result is consistent with the Laplace law predicting that the capillary pressure inside the liquid ligament depends linearly on the liquid surface curvature. Numerically, the high-pressure build up inside the

ligament leads makes it increasingly difficult for the solver to provide an accurate flow solution. A closure model is therefore necessary to continue simulating the post pinch-off portion and bypass such computationally challenging point.

1.1.3 Bypassing singularity by threshold breakup: numerical tests

Before introducing the physics-based closure model in subsection 1.4, we verify our findings on singularity by numerical forcing breakup at a prescribed threshold to bypass the singularity and achieve simulation convergence.

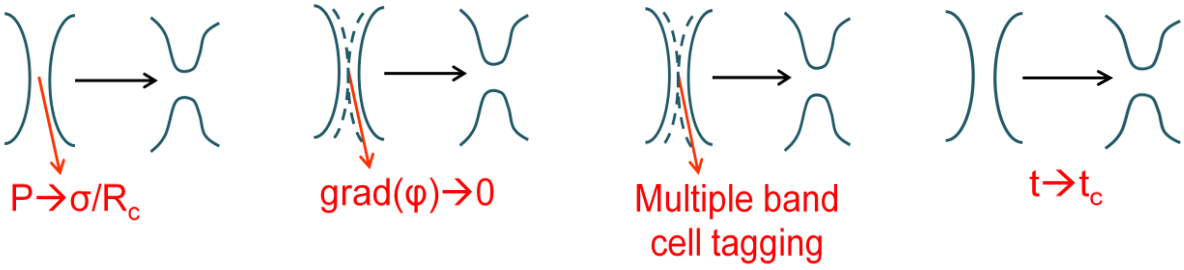

Figure 4. Different numerical approaches to introduce threshold breakup.

For the time being, the threshold is set for demonstration purposes and we do not apply any physical argument to determine its value. The most critical step in forcing breakup is to find the instant when the ligament reaches the prescribed threshold. Once the simulation reach this threshold length ℓ_f the state at the center of the ligament can be forced to change from liquid to gas by modifying the level set and volume of fluid functions. As shown in the schematics in Fig. 4, there are several different ways of defining ℓ_f and correspondingly different numerical approaches to force breakup.

The first approach, shown in frame (a), uses a value of critical pressure. For a thin cylindrical ligament, the pressure difference between liquid inside and gas outside is $\Delta P = \sigma / r$. When the ligament size reaches the threshold length ℓ_f, the pressure inside reaches a critical value $P_c = \gamma / \ell_f + P_g$, assuming the pressure in the gas phase P_g is constant. For each step in our simulation, we search for a location that has a global maximum pressure value. If the maximum pressure reaches the critical pressure P_c, we force breakup to occur at this location.

The second approach in frame (b) and the third approach in frame (c) are based on the level set geometric description of the interface. In the level set description, a distance function ϕ is used to define a field that has the interface embedded as the zero distance contours. Therefore, the distance to the interface is explicitly available at any location. A narrow-band with size $\ell_f / 2$ can be defined so that the distance from all the points within this band to the interface is less than $\ell_f / 2$. The thinning process of a ligament can be viewed as the $\ell_f / 2$-size band contracts and moves inward. When the band merge with itself at a certain location,

the size of the ligament is decreased to ℓ_f and the ligament is numerically forced to breakup. We found two numerical approaches to identify the location and instant for band merging. One as shown in Fig. 4(b) is to find a cell such that the module of the gradient of the level set function, $|\nabla\phi|$, significantly deviates from 1 (For a level set function defined by distance to a surface with radius of curvature larger than $\ell_f/2$, $|\nabla\phi|=1$ always holds). Another approach, shown in Fig. 4(c) is to find a cell that is tagged as a band cell for multiple times.

The fourth approach shown in Fig. 4(d) is the direct prescription of the pinch-off instant irrespective of the ligament state. This approach, requiring a-prior knowledge of the pinch-off location and therefore not applicable to a generic configuration, is expected to provide reference results with the least amount of numerical discrepancy at different resolutions.

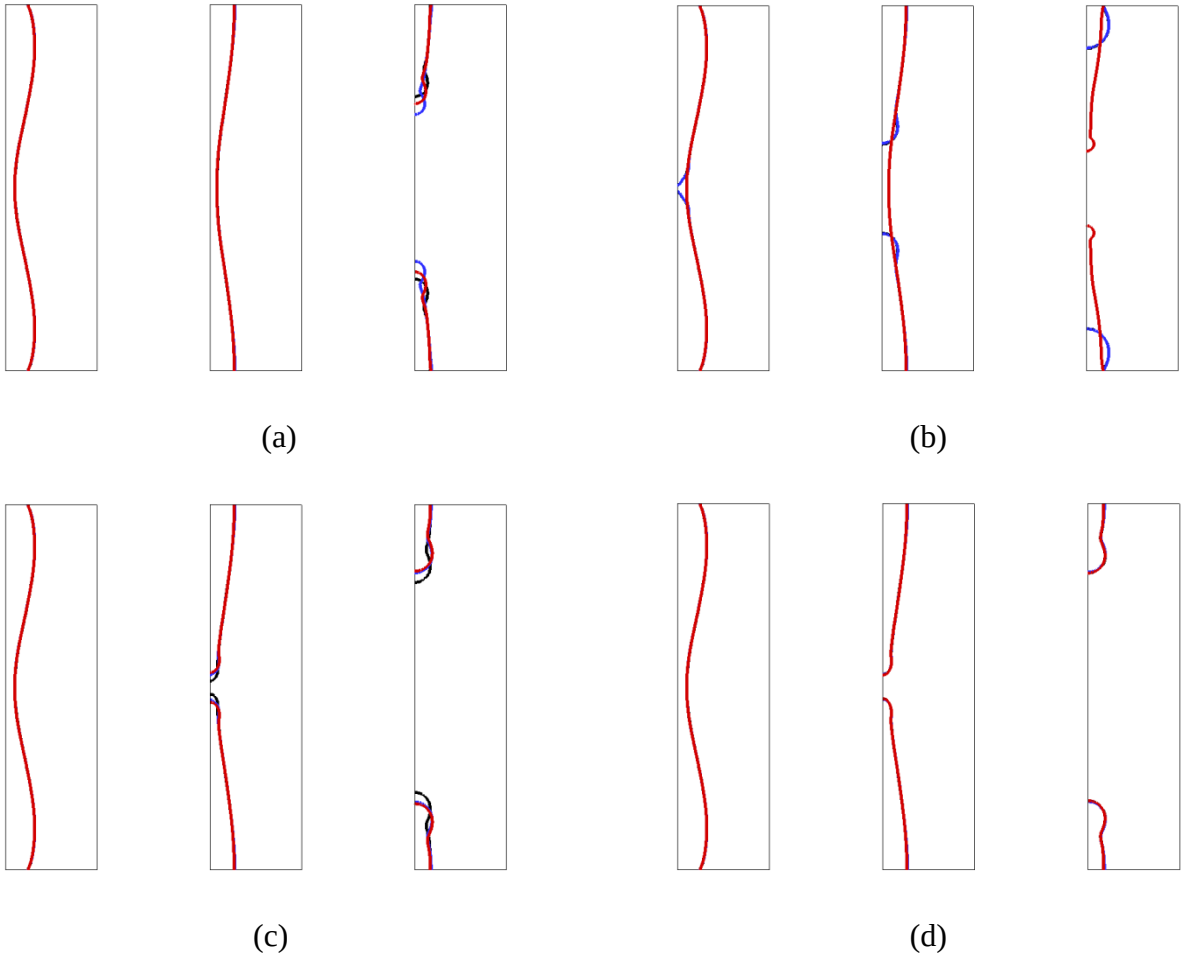

Figure 5. The interface location predicted at different resolutions using different threshold breakup approaches as in Fig. 4.

The interface location and maximum pressure for the straining case ($\dot{\gamma}=10^3\ \mathrm{s}^{-1}$) using the four different threshold breakup approaches are shown in Fig. 5 and Fig. 6 respectively. Results from different refinement levels are shown together in the same plots. Compared to Fig. 3 (b) and (d), all the threshold approaches predict much less discrepancy between simulations at different resolutions near and post pinch-off. Due to the numerical

approximation involved in computing the threshold pressure, the level set gradient and level set band width near the pinch-off location, different approaches reflected different type of sensitivities to the grid resolution. Even if using the same ligament width threshold, the level set gradient approach in frame (b) and the multi-band cell tagging approach in (c) predict different convergence behaviors. As expected, the pinch-off time prescription in (d) predicts the least amount of discrepancy between different resolutions.

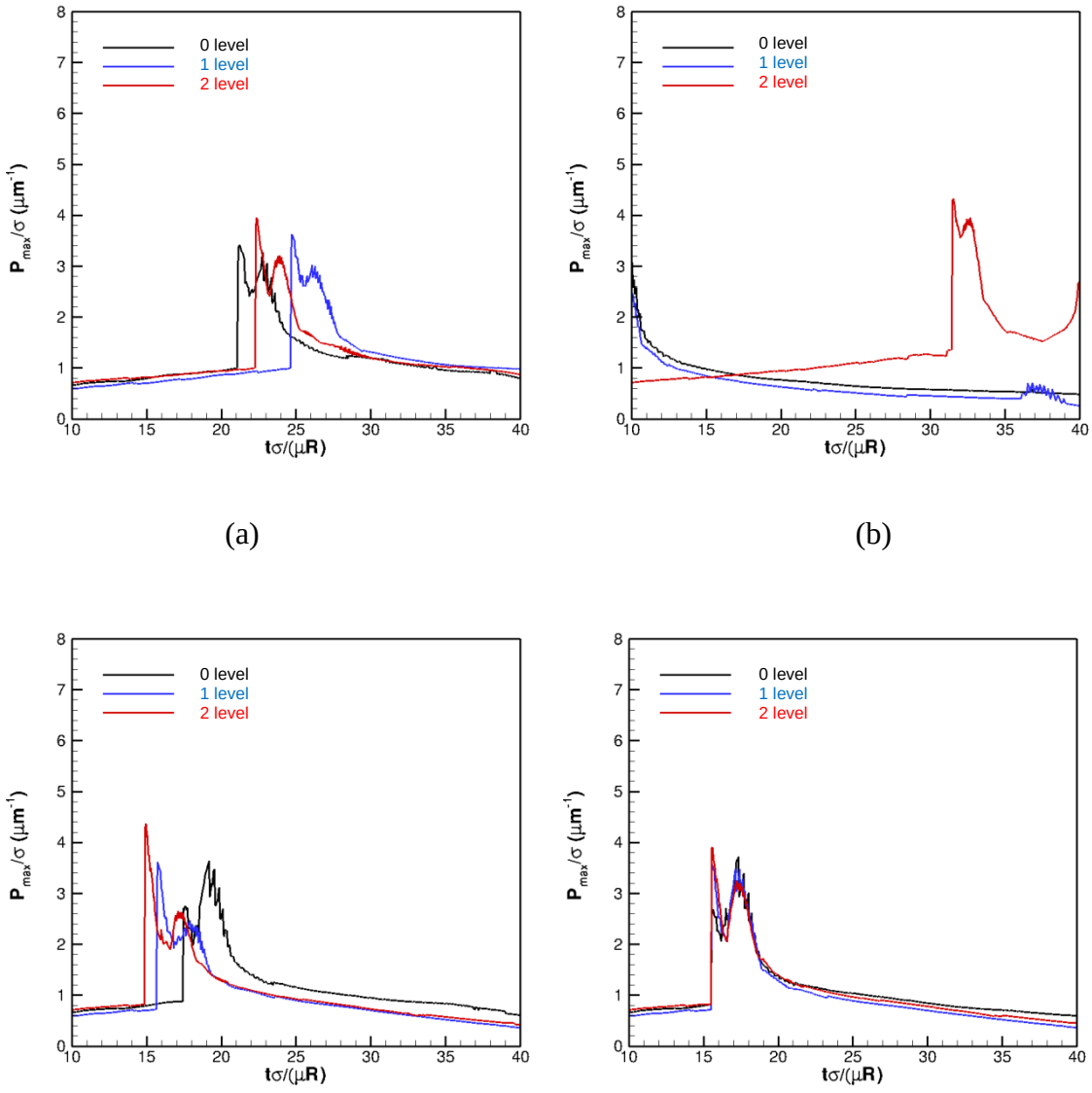

Figure 6. The maximum pressure at the pinch-off location at different resolutions using different threshold breakup approaches as in Fig. 4.

The threshold breakup tests discussed above verified that the reason for simulation divergence is the singularity present at the pinch-off instant. Bypassing the singularity can effectively provide a grid-converged simulation. However, the remaining question is how to

develop a mathematically/physically consistent model in order to bypass the pinch-off singularity and still accurately capture the process post pinch-off. This motivates the development of a meso-scale approach to achieve a detailed understanding of the pinch-off physics.

1.2 Development of a singularity-free meso-scale simulation approach

As shown in the previous section, numerical convergence near liquid pinch-off is difficult to achieve due to the singular nature of the continuum formulation. Physically, the effects of molecular scale fluctuations, which are averaged out in the continuum formulation, start to play a critical role near pinch-off. To correctly account for all the physics, a new model needs to be developed to incorporate molecular-scale information. Doing so in the continuum framework is challenging because the framework is established on the Navier-Stokes equations based continuum assumption. Particle based approach such as molecular dynamics can directly capture the molecular events, but at a prohibitively high cost. In this project, the mesoscopic Dissipative Particle Dynamics (DPD) approach is adopted to bridge the molecular and continuum scales. The interfacial dynamics is accounted for using a variant of DPD called Many-body DPD described below.

1.2.1 Background of MDPD

The advantage of dissipative particle dynamics (DPD) resides in the simplicity of the underlying algorithm of particle interaction under a soft repulsive potential. It has been shown that DPD can be constructed as a mesoscopic model of molecular dynamics (MD) [6], where the coarse-graining of Lennard-Jones clusters can lead to a suitable DPD force field. This result holds at sufficient low densities and for small ranges of gyration, when many-body effects can be neglected.

DPD has been used to investigate phase separation in immiscible binary liquid mixtures [7]-[9] droplet deformation and rupture in shear flow [10], and droplets on surfaces under the influence of shear flow [11]. In single-species fluid problems, however, the standard DPD method presents a fundamental limitation, in that the repulsive soft potential alone cannot reproduce surface tension. This potential leads to a predominantly quadratic pressure-density equation of state (EOS) [12], while a higher-order pressure-density curve is necessary for the coexistence of the liquid and vapor phases.

The free energy of the DPD system was modified by Tiwary and Abraham [13] to include a correction directly derived from the van der Waals EOS. The new term added the long-range attractive force that is responsible for surface tension between the liquid and the vapor phase; surface tension emerges from the asymmetry of the intermolecular forces acting on a layer of molecules at the liquid-vapor interface. As this asymmetry causes larger intermolecular

distances in the outer layer than in the liquid bulk, the forces in the layer act to contract the interface.

The many-body DPD (MDPD) method by Pagonabar-raga and Frenkel [14] also included an attractive force. The amplitude of the soft repulsion was made proportional to the local density of the particles, thus achieving a cubic pressure-density relation. A similar approach was introduced by Nugent and Posch in the context of smoothed particle hydrodynamics (SPH) [15]. The connection between MDPD and SPH was then clarified by Español and Revenga [16], who introduced a smoothed DPD (SDPD) method as a SPH variant based on a new formalism developed for discrete hydrodynamics [17].

MDPD was extensively investigated by Warren [18] and Trofimov *et al.* [19]. The method can be used for the study of single species free-surface flow, for instance, in the case of pinch-off of a liquid thread during the formation of a drop. There, the vanishing liquid thread diameter induces a singularity in the hydrodynamic description of a two-phase flow interface that is at odds with the continuum description of surface tension as a taut membrane of zero thickness. However, the focus of past research has been mostly on bulk properties, namely, the pressure-density relation [18]. This project focuses instead on the interfacial behavior of the MDPD fluid, on the sensitivity of the surface tension coefficient σ to the particle interaction parameters, and on the comparison with the properties of real liquids.

In the following, an extensive set of simulations is presented for a liquid with number density ρ in coexistence with a very dilute vapor. The dependence of σ from ρ is investigated based on a table of representative interaction parameters. An approximate mean-field expression is derived to directly evaluate the surface tension coefficient from the interaction parameters. The simulation of liquid thread pinch-off is then verified using analysis results derived in the limit of a slender jet.

All the simulations are enabled by the particle dynamics software code LAMMPS (Large-scale Atomic/Molecular Massively Parallel Simulator) [20] with the addition of a new MDPD class. The computationally scalable implementation of LAMMPS guarantees the optimization of the particle interaction calculation through an efficient neighbor list algorithm, and will not be discussed in this work.

1.2.2 Numerical details of MDPD

MDPD inherits the three pairwise-additive inter-particle forces formulation of the standard DPD scheme, $\mathbf{F}_i = \sum_{i \neq j} \mathbf{F}_{ij}^C + \mathbf{F}_{ij}^D + \Delta t^{-1/2} \mathbf{F}_{ij}^R$, with Δt the simulation time step. The conservative, dissipative, and random forces of this expression are defined, respectively, as

$$\mathbf{F}_{ij}^C = F_{ij}^C(r_{ij})\hat{\mathbf{r}}_{ij},$$

$$\mathbf{F}_{ij}^D = -\gamma \omega_D(r_{ij})(\mathbf{v}_{ij} \cdot \hat{\mathbf{r}}_{ij})\hat{\mathbf{r}}_{ij},$$

$$\mathbf{F}_{ij}^R = \xi \theta_{ij} \omega_R(r_{ij})\hat{\mathbf{r}}_{ij},$$

where $\hat{\mathbf{r}}_{ij} = \mathbf{r}_{ij} / r_{ij}$ and $\mathbf{v}_{ij} = \mathbf{v}_i - \mathbf{v}_j$. Warren's approach [18] is pursued for $\mathbf{F}_{ij}^C$; the repulsive force depends on a weighted average of the local density, whereas the attractive force is density-independent,

$$F_{ij}^C = A_{ij} w_c(r_{ij}) + B_{ij}(\bar{\rho}_i + \bar{\rho}_j) w_d(r_{ij}).$$

The weight functions $w_c(r) = (1 - r/r_c)$ and $w_d(r) = (1 - r/r_d)$ vanish for $r > r_c$ and $r > r_d$, respectively. Since a DPD method with a single range may not have a stable interface, the repulsive contribution is set to act at a shorter range $r_d < r_c$ than the soft pair attractive potential.

The many-body repulsion is chosen in the form of a self-energy per particle which is quadratic in the local density, $B_{ij}(\bar{\rho}_i + \bar{\rho}_j) w_d(r_{ij})$, where $B > 0$. The density for each particle is defined as

$$\bar{\rho}_i = \sum_{j \neq i} w_\rho(r_{ij}),$$

and its weight function w_ρ is defined as

$$w_\rho(r) = \frac{15}{2\pi r^3}(1 - r/r_d)^2$$

w_ρ vanishes for $r > r_d$ and for convenience is normalized so that $\int d^3\mathbf{r} w_\rho(r) = 1$.

The DPD thermostat consists of random and dissipative forces. The θ_{ij} coefficients are independent identically distributed Gaussian random numbers with zero mean and unit variance. The equilibrium temperature T is maintained through the condition posed by the fluctuation-dissipation theorem

$$w_D(r) = [\omega_R(r)]^2,$$

$$\xi^2 = 2\gamma k_B T,$$

where k_B is the Boltzmann constant. The weight function for the dissipative force is

$$w_D(r) = (1 - r/r_c)^2.$$

All the simulations presented in this report are carried out with the velocity Verlet algorithm of Groot and Warren [21] using the value 0.5 for the empirical parameter.

Dissipative particle dynamics methods operate in reduced units, such that energy is measured in units of k_BT; length in units of r_c, and mass in units of mass of a single particle, m. In the following discussion, we will find it convenient to refer to dimensionless quantities such as the Ohnesorge number and the Bond number.

1.2.3 Application to liquid-vapor interface dynamics

The operational expression to calculate surface tension at liquid-vapor equilibrium uses the macroscopic normal and tangential pressure values, or, alternatively, a perturbation formalism where surface tension is expressed as the energy difference between a reference state and a state with an infinitesimal area variation. Reference [21] compares the thermodynamic and mechanical routes for MDPD. We examine here the simplified relation that is established between the pressure difference ΔP across the liquid-vapor interface and the shape of a capillary surface according to the Young-Laplace equation (Y-L),

$$\Delta P = \sigma(\frac{1}{R_1} + \frac{1}{R_2})$$

In this expression, R_1 and R_2 are the principal radii of curvature of the surface. The Y-L relation is deduced from mechanical stability, and it has been shown to hold even for nanometer-size bubbles [23]. The internal pressure of a liquid can be calculated from

$$p^{virial} = \frac{\rho}{3}\left\langle (\mathbf{v} - \bar{\mathbf{v}})^2 \right\rangle + \frac{1}{6V}\left\langle \sum_{i \neq j} (\mathbf{r}_i - \mathbf{r}_j) \cdot \mathbf{F}^c_{i,j} \right\rangle ,$$

where $\langle\ \rangle$ denotes the sample average of the particles contained in the volume V and **v** is the sample velocity after being spatially averaged on V. The first term on the right-end side represents the thermal agitation of the molecules of the system. The second term is due to the interaction potential.

By way of illustration, drops with different diameters are simulated from an initial spherical lattice of particles in a box with periodic boundary conditions. The size of the box ensures that the drop is isolated. The initial random velocity distribution is at k_BT = 1. This value is maintained in the simulation by fixing the parameters ξ = 1 and γ = 0.5. The virial pressure at equilibrium is plotted in Fig. 7 as a function of radius for the set A = −40, B = 25, r_c = 1, r_d = 0.80. In this exercise there is no change in coarse-graining when the droplet radius is varied from one simulation to the next.

In examining the diagram in Fig. 7(a), it is apparent that the thermal contribution of the virial pressure is constant over most of the drop and that the plateau value is ρk_BT (the number density is 4.76). At the liquid-vapor surface, the thermal contribution decreases to zero within approximately one unit length. It can be shown that the actual extent of this transition region depends on the temperature of the drop and becomes larger at higher temperatures. The conservative term in Fig. 7(b) has a more complex behavior. Past the fluctuations near the droplet center, this term reaches a constant value when the number of sampled particles becomes sufficiently large.

The negative dip at the drop surface can be attributed to the strengthening of the attractive force as outward layer particles on average possess a larger inter-particle distance compared to the bulk particles. Further away, the longer-range attractive force vanishes, the virial pressure

becomes less negative, and it eventually goes to zero when the average inter-particle distance is larger than r_c.

The sum of the conservative and thermal terms forms the overall pressure field and is displayed in Fig. 7(c). The difference between the normal and the tangential component of the spherical interface is displayed in Fig. 7(d). For clarity, the diagrams from the smallest of the three droplets are omitted in this figure. The positive peak at the drop interface, followed by noise in the bulk (also omitted for clarity), illustrates the non-hydrostatic nature of the virial stress tensor that is responsible for surface tension. This diagram is consistent to what has been observed in molecular dynamics simulations for a Lennard-Jones fluid in a slab geometry [24].

The surface tension coefficient can be calculated directly according to the Y-L relation from the slope of the lines fitting the values of AP at various diameters; see Fig. 8. It is noted that this is not the only methodology to evaluate σ and that a more complete discussion can be found, for instance, in Refs. [13] and [21]. The radius of curvature of the drop is determined from the point where the number density falls below half of the bulk density value. This is a relatively precise measurement given the steepness of the interface at this temperature. The internal pressure is taken from the virial plateau value, with an uncertainty of ±0.4 for the smallest droplets and of less than ±0.002 for the largest drops in the range considered here. The MDPD parameters and the corresponding values of σ are listed in Table I. The values found for Sets 2 and 7 are in close agreement with the values reported in Ref. [18] (4.95 and 7.54) for the same parameters.

Set	A	B	r_d	ρ	σ	σ_{fit}
1	−40	40	0.80	3.94	1.90	3.33
2	−40	40	0.75	5.12	4.69	5.63
3	−30	25	0.75	5.27	3.51	4.48
4	−40	80	0.70	5.47	6.89	6.36
5	−50	40	0.75	5.60	8.42	8.43
6	−30	20	0.75	5.80	4.48	5.44
7	−40	25	0.75	6.10	7.30	8.02
8	−40	40	0.70	6.51	10.2	9.11
9	−40	20	0.75	6.77	9.14	9.90
10	−40	25	0.70	7.82	14.7	13.2

TABLE I. Parameter sets and properties of MDPD fluids. The bulk density ρ and the surface tension coefficient σ are calculated for $k_BT = 1$.

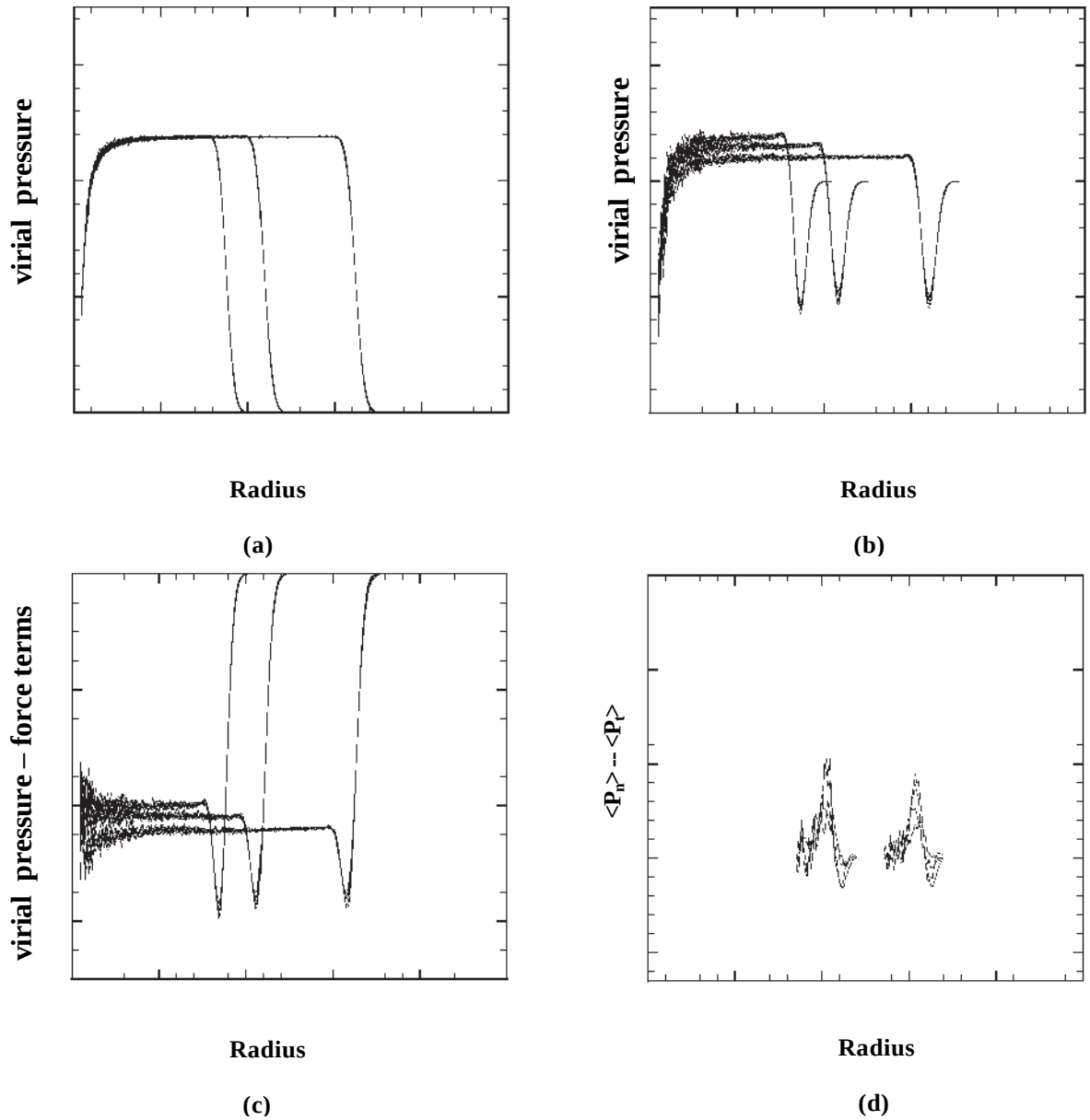

Figure 7. Virial pressure as a function of radius for three drops of fluid 1 (the interaction parameters are listed in Table I): (a) contribution of thermal motion; (b) contribution of the conservative forces (c) resulting virial pressure; (d) radial minus tangential component of virial pressure.

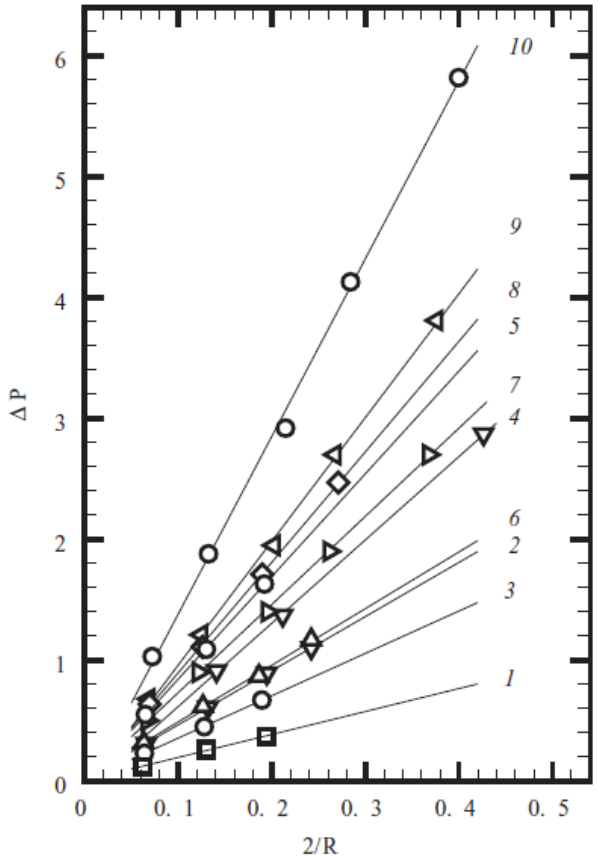

Figure 8. Pressure difference across the liquid-vapor interface of a drop in equilibrium versus its curvature for the 10 MDPD fluids listed in Table I.

The occurrence of capillary pinch-off has already been demonstrated by a modified DPD method [24] as well as by pioneering molecular dynamics simulations [26]. Here, we examine whether MDPD captures the correct fluid dynamic behavior by assessing the response of a quiescent circular jet of diameter D to a periodic axial perturbation. It is well known that the jet becomes unstable if $\lambda/D > \pi$ [27]. Above that cutoff wavelength, the cylinder surface is driven toward the state with the smallest area, and, locally, to pinch-off. In this process, the greater the cohesion between the particles (and thus the surface tension), the faster the instability develops. Below the cutoff, surface tension has the opposite role of restoring the jet to its unperturbed state. In the inviscid description of the Plateau-Rayleigh instability [28], linear analysis of perturbation leads to the maximum growth of a disturbance for $\lambda/D \sim 4.5$. By dropping viscosity from dimensional analysis, the characteristic pinch-off time is

$$\tau = \sqrt{\rho D^3 / \sigma}$$

As a demonstration, simulations are carried out for two jet diameters in a 10^3 box with periodic boundary conditions and sinusoidal perturbation of wavelength $\lambda = 10$. The MDPD parameters correspond to Set 2 in Table I. The random and dissipation coefficients are $\xi = 12$ and $\gamma = 72$; the time step is $\Delta t = 0.001$.

In the first simulation, we set L/D = 4.5 with 251 particles. Fig. 9(a) displays a sequence of snapshots as seen through a slice of the jet. Initially, the amplitude of the perturbation is only

one layer of particles. The jet begins to neck at around t = 2.7 and pinches off soon thereafter, so that by t = 13 the two half droplets have fully equilibrated. The characteristic time is τ = 3.46. The actual time to pinch-off depends on the seed values that are used to generate random numbers for the stochastic force and for the initial velocity distribution. It is, however, well defined in every realization of this case.

In the second simulation, the diameter is increased to D = 5, with 1116 particles. No capillary instability develops, even for large amplitude perturbations, and the jet returns to a cylindrical shape under the restoring force of surface tension. The simulation can continue for a very long time (the last frame of Fig. 9(b) shows a snapshot at t = 200) without pinch-off ever occurring. This and the previous result are consistent with the Plateau-Rayleigh analysis.

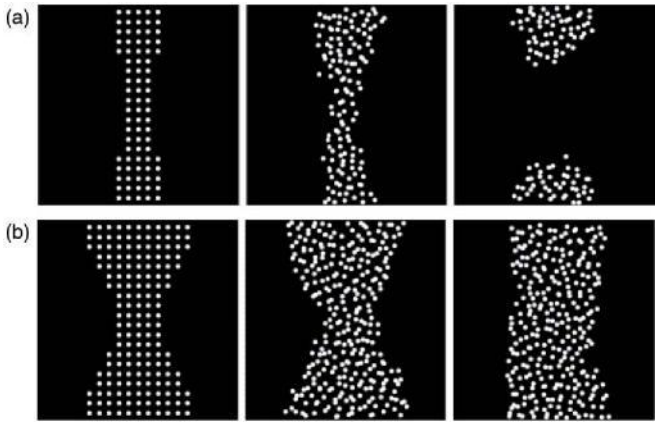

Figure 9. Snapshots of capillary dynamics of a liquid thread: L/D = 4.51 (top) and L/D = 2.5 (bottom).

1.2.4 Non-periodic boundary conditions

A novel element in this study is the implementation of a Non-Periodic Boundary Condition (NPBC) to broaden the application of particle methods and study straining gas-liquid fields. A first challenge is that the boundary conditions need to include the right amount of attractive force, responsible for the continuity of the liquid. Implementation of a simple reflecting wall alone is not sufficient because there would not be any force anchoring the MDPD boundary particles. Also, an effective-force approach where potential is applied to impose the desired kinematics is insufficient to keep the liquid and gas phase separated.

As shown in the schematics of Fig. 10, two layers of particles are built into the domain on each side of the computational box where the NPBC is assigned. The outermost layer (O) is modified at every iteration by placing particles of the prescribed type. This layer is a fixed (no time integration) barrier whose composition depends on the instantaneous location of the boundary interface. Layer (O) provides the necessary attractive force for the continuity of the MDPD liquid.

Particles from the innermost (I) layer of the buffer are free to move according to the distribution of the surrounding particles. At the end of every iteration their velocity is modified so that 1) the average particle velocity of a cell of the buffer matches the prescribed velocity of that buffer; 2) the squared deviation from that average value matches the prescribed temperature. Here, "cell" refers to an element of volume of side $L_i = n_i^{-1/3}$, where n is the number density of component i; see Fig. 10. Particles are free to cross in both directions the boundary between the (I) layer and the domain proper, but particles crossing the separation between layers (I) and (O) are reflected back. This wall moves at the velocity of the normal component of $\mathbf{v}_b$.

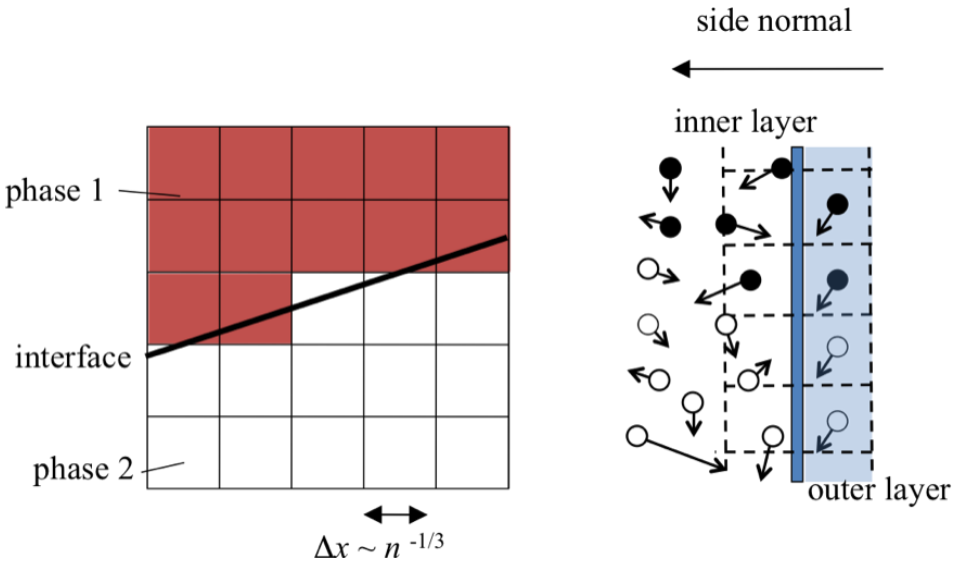

Figure 10. Schematics showing the prescription of composition and velocity at a face boundary.

A numerical test discussed here is the enforcement of the extensional configuration displayed in Figure 2, with minimum radius of the dumbbell R = 6.5. The flow field is achieved by imposing NPBCs on the sides of a 50^3 box. The domain initially contains 14,512 particles of liquid and 15,924 particles of gas. The liquid particles have the properties listed above; the gas particles are treated as DPD particles (no attractive force): A = 10, r_c = 1, B = 0, r_d = 0.75; γ = 288, and ξ = 24. These parameters correspond to ν = 0.84 and n = 1.2. To obtain a liquid/gas density ratio of 780, the mass is set to m = 0.0064.

The time-averaged velocity of the particles arranges itself quickly to a fully developed extensional field. As time progresses, liquid particles exit the domain while more gas particles enter it. To account for the advection component involved in imposing a prescribed strain rate, the time step is set to 0.00004 in DPD units. Thus, a calculation including the interaction with the gas phase is substantially more expensive than the single-component simulations of capillary pinch-off discussed earlier. Also, NPBCs require two additional layers of particles for each boundary pair – a 12% increase in the overall system size. Fig. 11 shows an excellent agreement with the corresponding CLSVOF simulation at three instants preceding pinch-off.

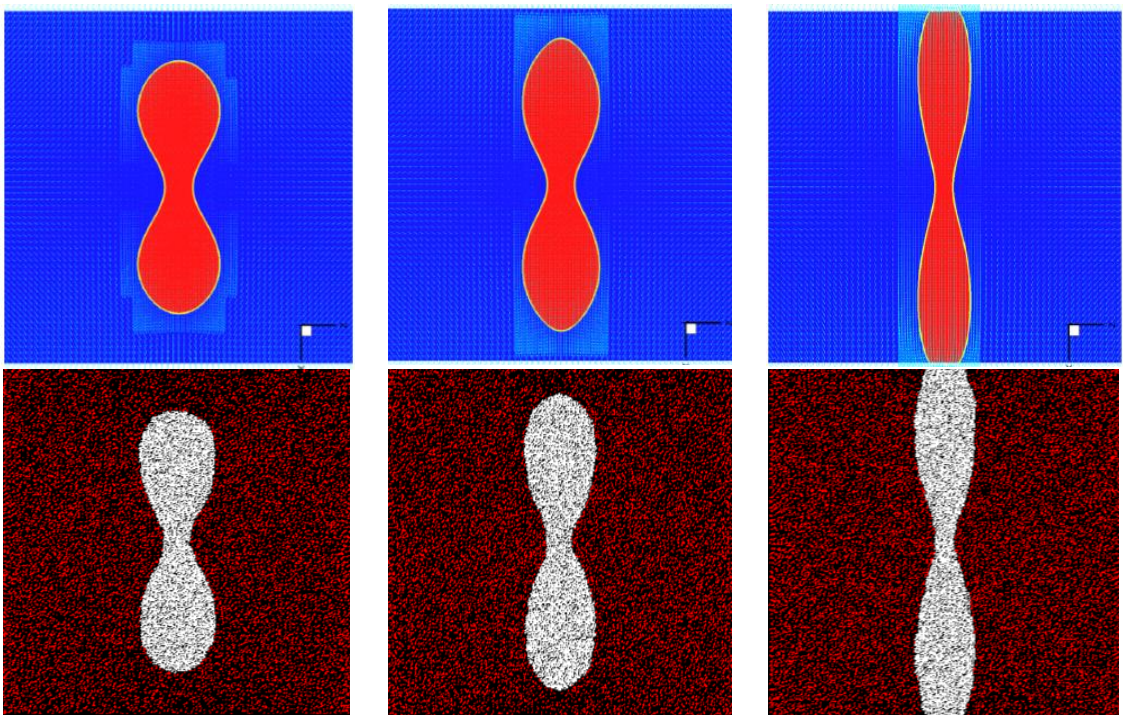

Figure 11. Axis-symmetric dumbbell subject to extensional flow: CLSVOF (top) and MDPD (bottom) snapshots before pinch-off.

1.3 Scaling analysis of pinch-off using meso-scale simulations

1.3.1 Theoretical background of pinch-off scaling

Theoretical description of interface dynamics when a liquid thread shrinks to zero near pinch-off – and interface curvature goes to infinity – has been rare in the literature. A notable exception is Eggers' similarity solution derived for drop pinch-off in free-surface flow [29]. It is shown that pinch-off at ($\mathbf{x}_0$, t_0) is a singularity of the Navier-Stokes equations in a critical region $|\mathbf{x}'| << 1$ and $t' << 1$, where

$$\mathbf{x}' = \frac{\mathbf{x} - \mathbf{x}_0}{\ell_\nu} \qquad \text{and} \qquad t' = \frac{t - t_0}{\tau_\nu}.$$

The parameters ℓ_ν and τ_ν depend only on the property of the liquid,

$$\ell_\nu = \left(\rho\nu^2\right)/\sigma \qquad \text{and} \qquad \tau_\nu = \left(\rho^2\nu^3\right)/\sigma^2,$$

with ν, ρ, and σ are the liquid viscosity, density and surface tension, respectively. For water (ρ = 1000 kg/m^3; ν = 1.138 10^{-6} m^2/s; σ = 0.0728 N/m), these viscous length (ℓ_ν = 1.77 10^{-8} m) and time (τ_ν = 2.78 10^{-10} s) scales are very small compared to scales in most continuum simulations. An important consequence of Eggers' work is that the minimum liquid thickness along the ligament scales linearly with the time left to the singularity time t_0,

$$h_{min} = 0.03\frac{\sigma}{\rho\nu}\left(t - t_0\right),$$

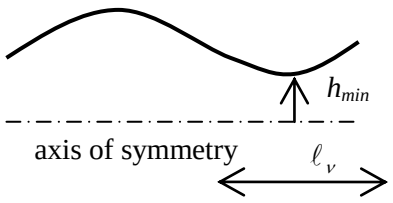

Figure 12. Sketch of the flow geometry investigated by Eggers [29].

Another analytical work by Lister and Stone [3] applied the asymptotic balance between surface tension and viscous stress,

$$\sigma/h_{min} \sim \rho u \nu / h_{min},$$

which also suggest the thinning rate of the thread u becomes asymptotically constant in time,

$$u \sim \sigma/(\rho\nu)$$

and pinching-off occurs with a finite period. All the work suggests that Navier-Stokes equation is singular at the point of pinch-off and it has a self-similar solution in the limit of the singularity. The solution is universal, in the sense that it is independent from the particular initial or boundary conditions of the experiment.

The physics of liquid pinch-off is in fact more complex than that described by Navier-Stokes equations. Intuitively, it can be expected that when the liquid thread thickness is comparable to the scale of thermal fluctuations that are averaged out in the continuum description – or to the actual interface width (~100nm) – the Navier-Stokes description of two-phase flow breaks down. For liquid, the thermal length scale,

$$\ell_T = (k_B T / \sigma)^{1/2},$$

accounts for the fact that molecules at the interface have energies due to both thermal motion and surface tension. ℓ_T is of the order of a nanometer in most fluids at room conditions. In free surface flow, a threshold length exist,

$$\ell_{thres} \sim \ell_\nu \left(\frac{\ell_T}{\ell_\nu} \right)^{2/5},$$

below which thermal capillary instabilities can cause the interface to behave stochastically. For fuel at ambient temperature, ℓ_{thres} = 1 μm, which is comparable to the thickness of the liquid thread that forms before pinch-off.

The domain concerned by thermal fluctuations (up to a few hundreds of nanometers) has been recently probed by Molecular Dynamics (MD) simulations. MD simulations of nanojets show a substantial change in behavior near pinch-off [30]. This behavior is predicted by the stochastic lubrication equation (SLE) [26], derived from the Navier-Stokes equations in the limit of a slender jet and with the addition of Gaussian noise to the deterministic stress tensor. The relation between h_{min} and $t_0 - t$ is described by a power law with exponent 0.418, found by numerical integration [31].

1.3.2 MDPD scaling analysis for capillary pinch-off

To establish a connection with the theory, the results from previous MDPD simulation of dumbbell drop breakup by capillary effects (subsection 1.2.3) are post-processed and the minimum thread radius h_{min} are plotted as a function of the time to breakup, $t_0 - t$ in Fig. 13. The time to pinch-off in Fig. 13 is normalized by τ, whereas h_{min} is normalized by the unperturbed jet radius R. To track the minimum jet radius, it is necessary to post-process several snapshots of particle positions, each axially sliced into 50 bins. It is assumed that the only 1% or less of the particles lie outside the surface of the jet, a threshold consistent with almost no vapor phase. The jet radius, calculated with respect to the instantaneous position of the center of mass in each slice, is defined based on the radial histogram of number density. The pinch-off time is established as the instant when one of the bins becomes empty. The simulation is carried out in a 80^3 periodic cube using the parameter set 7 from Table I for a system of 118,657 particles; the time step is Δt = 0.001. The dissipation and random

coefficients are σ = 0.5 and ξ = 1, giving ν = 0.072; the Ohnesorge number is therefore Oh = 0.022.

The logarithmic plot of $h_{min}(t_0 - t)$ in Fig. 13 demonstrates that a single MDPD simulation can span the three scaling behaviors listed above. Initially, and for almost a time decade, the tracked points are aligned along the 2/3 slope. The inertial-viscous behavior appears at approximately $h_{min}=0.3R$ and is quickly overtaken by a trend where most of the points align along the slope 0.418. This occurs approximately at $h_{min}=0.15R$, above the thermal capillary length $l_T = 0.042\ R$. At that point, as noted by Eggers [31], any random fluctuation which increases the thread radius will also increase its effective mass, slowing down the motion of the fluid; conversely, any fluctuation toward a smaller neck radius will accelerate pinch-off. The gap between deterministic hydrodynamics and molecular dynamics is thus bridged in this simple example. Other MDPD simulations (not shown here) confirm that a larger viscosity or a smaller domain causes the potential-flow scaling to disappear from the diagram.

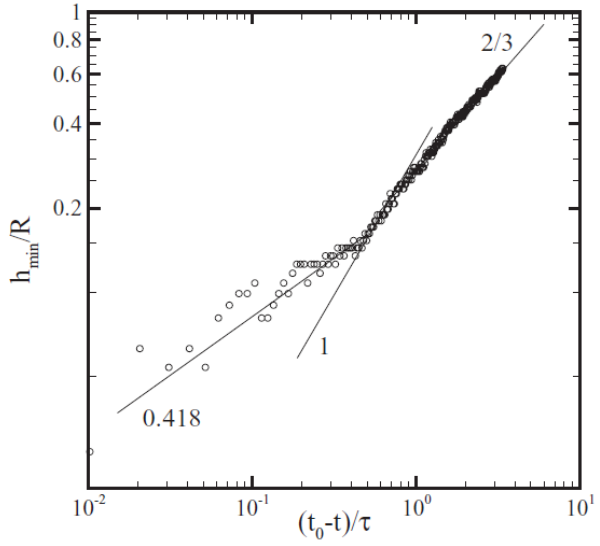

Figure 13. Variation of minimum thread radius h_{min} versus time to breakup $t_0 - t$. The three lines correspond to potential flow (slope 2/3), inertial-viscous (slope 1), and stochastic (slope 0.418) power laws. The open symbols are measured values from the MDPD simulation.

1.3.3 MDPD scaling analysis for pinch-off in straining flow

To simulate pinch-off of drop in a straining flow using MDPD, Non-Periodic Boundary Conditions (NPBCs) is implemented at the boundaries of the simulation domain. As time progresses, liquid particles exit the domain while more gas particles enter it. The number density, mass and viscosity of these two fluids are arranged so that the gas-liquid density ratio is 0.0013, and that the kinematic viscosity ratio is 15. These two values are in the range of typical air/liquid ratios for air at ambient conditions.

The straining case presented in subsection 1.1.2 was simulated using MDPD. Several snapshots for the simulations at two different strain rates are shown in Fig 14. The time is

scaled by DPD unit time. As the strain rate increases, the global-scale elongation of drop becomes faster. However, closer look at the local-scale neck region (rectangular box) reveals that the local pinch-off process does not depend much on the strain rate. At the same time t-t_0 relative to pinch-off, the thread shapes are quite similar for the two strain rate cases even though the larger-scale drop shapes are different.

The minimum thread radii h_{min} under the two strain rates are extracted from the simulation and plotted as a function of time in Fig. 15. The two cases show certain degree of discrepancy due to the molecular-scale fluctuations when pinch-off is approached. However, h_{min} for both cases shows the same transition from inertial scaling to inertial viscous scaling and to stochastic scaling. The point of transition seems agree as well for the two cases. The results suggest that strain rate does not affect the evolution of thread neck near pinch-off. As pointed out by Eggers [29], the thread behavior approaching pinch-off becomes self-similar and depends only on intrinsic length and time scales, independent of external conditions such as strain rate. The results in Fig. 15 agree with such theoretical arguments. The theoretical argument also suggests that the transition point between inertial and viscous scaling is only dependent on the fluid properties (such as density, viscosity and surface tension) and independent of strain rate. Such condition-independent transition point separates the physics occurring in different scales. At a scale above the transition point, strain rate affect larger scale two-phase flow (see Fig. 14). At a scale below the transition point, the physics is independent of strain rate and only affected by molecular-level fluctuations. It can also be inferred that because of the scale separation, the molecular fluctuation does not impact larger scale dynamics.

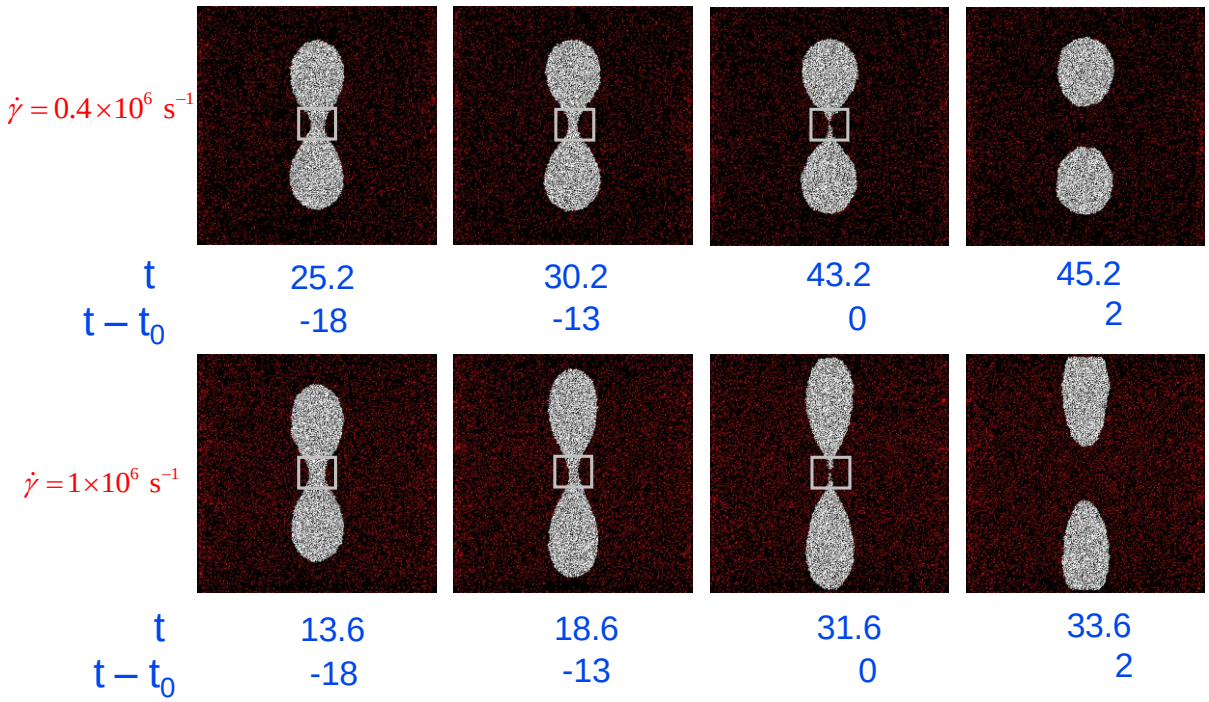

Figure 14. Snapshots of dumbbell drop breakup in a straining flow at different strain rate: $\dot{\gamma} = 0.4\times10^{6}\ s^{-1}$ (top) and $\dot{\gamma} = 10^{6}\ s^{-1}$ (bottom).

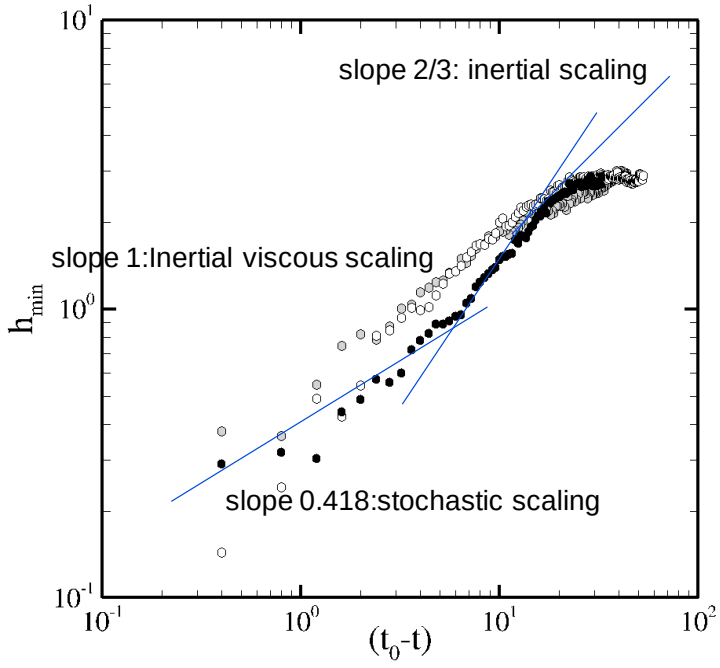

Figure 15. Variation of minimum thread radius h_{min} versus time to breakup $t_0 - t$. for different strain rate: $\dot{\gamma} = 0.4 \times 10^6\ s^{-1}$ (circle) and $\dot{\gamma} = 10^6\ s^{-1}$ (dot).

1.4 Development and demonstration of continuum-scale closure model

1.4.1 Closure model development from scaling analysis

The analysis in subsection 1.3.3 gives rise to a key finding that allows developing a physics-based closure model for continuum simulations.

The simulation based on the continuum formulation can resolve the thread neck down to the inertial to inertial viscous scaling transition point. Because the process below the transition point is independent of external flow conditions, the transition point can be used as a universal threshold for certain liquid-gas pair with fixed fluid properties. The threshold is physics-based and independent of grid-resolutions. The value of the threshold can be obtained using meso-scale analysis such as MDPD simulations and applied in continuum simulations as the criterion to stop simulating the process below the transition point and introduce a numerically forced breakup. Because of the condition-independent nature of the threshold, same threshold for numerical breakup can be applied for any pinch-off processes occurring in the simulation domain irrespective of their local strain rate. The scaling transition point thus becomes the only parameter of the closure model.

In next subsection, a generic implementation of such closure model in CLSVOF framework will be described. A converged pinch-off simulation when the closure model is applied will be demonstrated.

1.4.2 Generic implementation of the closure model

Since a physics-based threshold has been determined as the scaling transition point, the implementation of the closure model involves developing a generic procedure to identify and cut the liquid in thread neck region that falls below the threshold.

The identification procedure is motivated by the algorithm for liquid filament identification proposed by Kim and Moin [4], but with substantial modifications to adapt to the current CLSVOF and AMR framework. The algorithm is illustrated in Fig. 16. First, all cells are grouped in gas phase ($\Pi < 0$), liquid phase ($\Pi \geq 0$), and liquid-gas interface ($\Pi \geq 0$ and directly adjacent to $\Pi < 0$), respectively. Then for each interface cell $\mathbf{x}_i$, its unit normal $\mathbf{n}_i$ is calculated as $\mathbf{n}_i = \nabla\phi/|\nabla\phi|$. With $\mathbf{x}_i$ and $\mathbf{n}_i$, a traverse line can be constituted that serves as the center-line of a three-dimensional cylinder traversing through the liquid phase in direction $\mathbf{n}_i$ with a radius r. Starting from the interface cell $\mathbf{x}_i$, all its immediate neighbors in the liquid phase are searched. If the location of a neighboring cell falls within the range of the cylinder, it is added into a list of cells. The next round search initiates from the immediate neighbors of the newly identified cells from the previous round, and is carried out in the way of a multi-branch tree search [5]. Note that the cells visited in one round of search are tagged such that a redundant search during the next round for these cells can be avoided. Eventually the search is stopped when none of the neighbors of the cells within the list can be found in liquid phase (including liquid-gas interface) and enveloped by the cylinder. Once the search is finished, the maximum distance from the initial interface cell $\mathbf{x}_i$ to another interface cell $\mathbf{x}_e$ in the list is

calculated. This distance represents the local liquid thread thickness in the direction $\mathbf{n}_i$. If it does not exceed the threshold pinch-off size, this list of cells is marked as valid candidate cells, which are labeled in green color in Fig. 16.

The above cylinder-envelope search procedure is carried out for each interface cell. As a result, all the cells meeting the criteria of liquid thread thickness are marked. The next step is to collect contiguous cells from the tagged ones into separate cell lists to represent separate liquid structures. This is achieved again by performing the multi-branch tree neighbor cell search described above. Note that the above algorithm is generic in the sense that any region with thickness below the threshold will be identified, irrespective the location and orientation of the region. The algorithm does not involve numerical computation of gradients, making it less sensitive to numerical perturbations. Also the algorithm can be applied in any dimensions.

After the potential liquid pinch-off structures are identified, they are constrained by an additional criterion: A liquid filament is disqualified if it contains any liquid cells that touch the boundaries of an AMR box. In other words, the ligament is not allowed to cross an AMR box and operations on the ligament are constrained within one local box. As a result, the breakup operation may be delayed in case the ligament does cross multiple boxes. This might seem arbitrary, but due to the dynamic features of AMR, the current box-crossing liquid structure has a good chance to be completely contained by a new box within a few time steps as the mesh refinement needs to be performed adaptively at every time step. In addition, it is advantageous to consider only the local box operation, such that the complexity of exchanging liquid structure information between boxes computed on different processors is avoided, thus the communication overhead is saved.

In the current model, the forced breakup occurs at a very small scale. It is thus reasonable to assume that the continuum simulation (CLSVOF algorithm) directly captures the small scale pinch-off between the smallest satellite drops. The resultant small amount of residual mass due to the forced breakup is considered negligible; albeit the mass should be redistributed back to the parent drops in the strict sense of mass conservation.

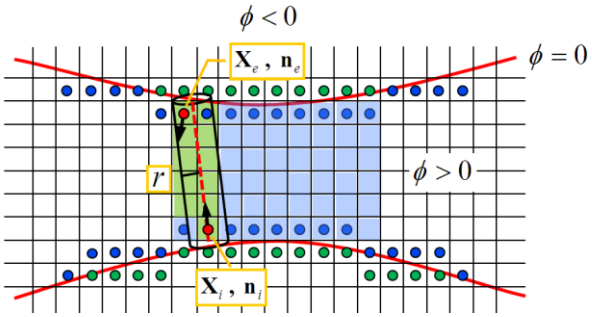

Figure 16. A schematic of the liquid thread identification algorithm.

1.4.3 Demonstration of simulation convergence using the closure model

With the closure model embedded in the continuum solver, a three-dimensional drop breakup in a straining flow is simulated at different resolutions (controlled via AMR). Although the flow is largely two-dimensional axisymmetric, we perform the simulation in the 3D version of the solver to test the generality of the closure model implementation. The cost of this demonstration is much higher than the test cases presented in subsection 1.1.2.

The physical length scale of the scaling transition point is on the order of micro meters. To have the continuum solver capture such small scales within affordable simulation time, we hereby perform the demonstration for the pinch-off of a small dumbbell drop of initial unperturbed cylindrical diameter $D = 8$ μm, wavelength $\lambda = 20$ μm, and wave magnitude $\varepsilon =$ 2μm. For water-air system, the physical scaling transition point is found to be 1.72 μm based on MDPD simulation results. The continuum simulations are performed in a 48 μm×48 μm×48 μm domain with coarsest resolution being used to be 96×96×96. The coarsest grid size is 0.5 μm, far below the threshold. That means the drop dynamics before the threshold is reached can be resolved by the simulation. The grid setup for refined cases is summarized below.

Case No.	Base grid	Refinement level	Refined grid size
1	96×96×96	0	0.5 μm
2	64×64×64	1	0.375 μm
3	96×96×96	1	0.25 μm
4	64×64×64	2	0.188 μm

The snapshots of simulations prior to, near and post pinch-off are shown in Fig. 17 with the results from different resolutions compared. By enforcing breakup at the same physics-based threshold independently from grid resolution, the simulation converges with decreasing Δx. The drop shapes match quite closely in the three refined cases with AMR (Δx = 0.375 μm, 0.25 μm, 0.188 μm). The post pinch-off shapes match each other at the same time instant. To quantitatively verify the convergence, the breakup time t_0 and the post pinch-off separation distance d_{sp} are extracted from the simulations and plotted as a function of grid size in Fig. 18. It is observed that both t_0 and d_{sp} reaches a constant value as the grid size decreases. The results clearly demonstrate the convergence of the calculation, which can finally be considered as a Direct Numerical Simulation of the flow.

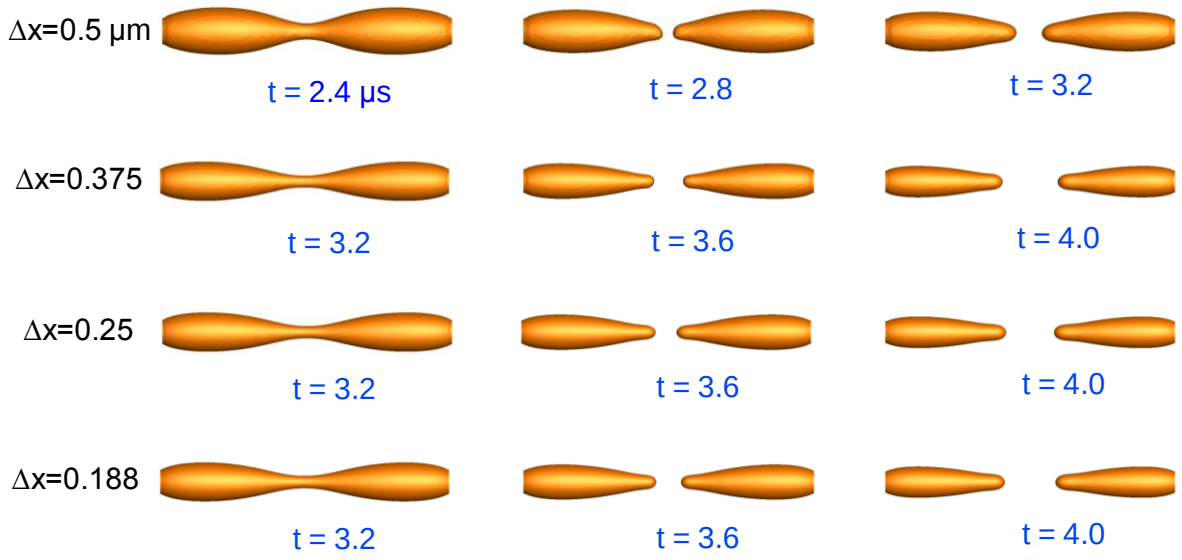

Figure 17. Snapshots of drop shape predicted by simulations at different resolutions using the physics-based closure model.

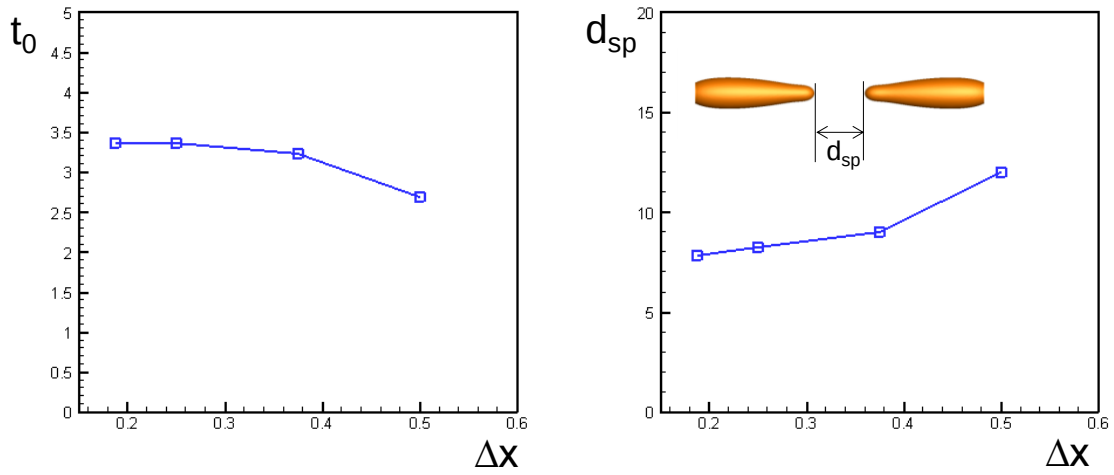

Figure 18. The grid convergence of pinch-off time (a) and drop separation distance post pinch-off.

Chapter 2

Personnel supported

Xiaoyi Li	2009-2010, Co-investigator
	2010-2012, PI
	Staff Research Engineer, United Technologies Research Center, East Hartford, CT
Marco Arienti	2009-2010, PI
	Staff Research Engineer, United Technologies Research Center, East Hartford, CT
	2010-2012, Co-investigator
	Staff Scientist, Sandia National Laboratory, Livermore, CA
Hui Gao	2011-2012, Co-investigator
	Senior Research Engineer, United Technologies Research Center, East Hartford, CT
Marios Soteriou	2009-2012, Co-investigator
	Research Fellow, United Technologies Research Center, East Hartford, CT
George Karniadakis	2009-2012, Consultant
	Professor, Brown University, Providence, RI
Mark Sussman	2009-2012, Consultant
	Associate Professor, Florida State University, Tallahassee, FL

Chapter 3

Publications and presentations

Journal papers

Marco Arienti, Wenxiao Pan, Xiaoyi Li, and George Karniadakis, "Many-body Dissipative Particle Dynamics simulation of liquid/vapor and liquid/solid Interactions", Journal of Chemical Physics 134 (20).

Xiaoyi Li, Marco Arienti, and Hui Gao, "A physics-based closure model for continuum simulations of two phase flow through pinch-off singularity", Journal of Computational Physics, to be submitted.

Conference papers and presentations

Marco Arienti, and Xiaoyi Li, "A mesoscale study of pinch-off under high strain", 12th International Conference on Liquid Atomization and Spray Systems, Heidelberg, Germany, September 2012.

Hui Gao, Xiaoyi Li, Marios Soteriou, and Marco Arienti, "Towards a physics-based model for numerical simulation through the pinch-off singularity", ILASS Americas, 24th Annual Conference on Liquid Atomization and Spray Systems, San Antonio, TX, May 2012.

Bibliography

[1] Sussman, M., Smith, K.M., Hussaini, M.Y., Ohta, M., and Zhi-Wei, R., Journal of Computational Physics 221: 469-505 (2007).

[2] A.S. Almgren, J.B. Bell, P. Colella, L.H. Howell, M. Welcome, Computational Physics, 142, 1–46, 1998.

[3] Lister, J.R., and Stone, H.A., Physics of Fluids 10: 2758-2764 (1998).

[4] Kim, D., and Moin, P., "Numerical Simulation of The Breakup of A Round Liquid Jet by A Coaxial Flow of Gas with A Subgrid Lagrangian Breakup Model," Annual Research Briefs, Center for Turbulence Research, Stanford University, 15-30 (2011).

[5] Li, X., Arienti, M., Soteriou, M.C., and Sussman, M., AIAA Aerospace Sciences Meeting, Orlando, FL., AIAA 2010-092407.

[6] H. Lei, B. Caswell, and G. E. Karniadakis, Phys. Rev. E 81, 026704 (2010).

[7] P. V. Coveney and K. E. Novik, Phys. Rev. E 54, 5134 (1996).

[8] S. I. Jury, P. Bladon, S. Krishna, and M. E. Cates, Phys. Rev. E 59, R2535 (1999).

[9] K. E. Novik and P. V. Coveney, Phys. Rev. E 61, 435 (2000).

[10] A. T. Clark, M. Lal, J. N. Ruddock, and P. B. Warren, Langmuir 16, 6342 (2000).

[11] J. L. Jones, M. Lal, J. N. Ruddock, and N. Spenley, Faraday Discuss. 112, 129 (1999).

[12] A. A. Louis, P. G. Bolhuis, and J. P. Hansen, Phy. Rev. E 62, 7961 (2000).

[13] A. Tiwari and J. Abraham, Phys. Rev. E 74, 056701 (2006).

[14] I. Pagonabarraga and D. Frenkel, J. Chem. Phys. 115, 5015 (2001).

[15] S. Nugent and H. A. Posch, Phys. Rev. E 62, 4968 (2000).

[16] P. Español and M. Revenga, Phys. Rev. E 67, 026705 (2003).

[17] P. Español, M. Serrano, and H. C. Ottinger, Phys. Rev. Lett. 83, 4542 (1999).

[18] P. B. Warren, Phys. Rev. E 68, 066702 (2003).

[19] S. Y. Trofimov, E. L. F. Nies, and M. A. J. Michels, J. Chem. Phys. 123, 144102 (2005).

[20] S. J. Plimpton, J. Comput. Phys. 117, 1 (1995).

[21] R. D. Groot and P. B. Warren, J. Chem. Phys. 107(11), 4423 (1997).

[22] A. Ghoufi and P. Malfreyt, Phys. Rev. E 82, 016706 (2010).

[23] M. Matsumoto and K. Tanaka, Fluid Dyn. Res. 40, 546 (2008).

[24] A. Trokhymchuk and J. Alejandre, J. Chem. Phys. 111, 8510 (1999).

[25] A. Tiwari and J. Abraham, Microfluid. Nanofluid. 4(3), 227 (2008).

[26] M. Moseler and U. Landman, Science 289, 1165 (2000).

[27] J. A. F. Plateau, Statique expérimentale et theorique des liquides soumisaux seules forces moléculaires (Gauthier Villars, Paris, 1873), Vol. 2.

[28] J. W. S. Rayleigh, Proc. R. Soc. 29, 7197 (1879).

[29] J. Eggers and E. Villermaux, Rep. Prog. Phys. 71, 036601 (2008).

[30] W. Kang, "Molecular dynamics simulations and microscopic hydrodynam-ics of nanoscale liquid structures," Ph.D. dissertation (Georgia Institute of Technology, 2008).

[31] J. Eggers, Phys. Rev. Lett. 89, 084502 (2002).

[32] Arienti, M. and Li, X., 12th International Conference on Liquid Atomization and Spray Systems, Heidelberg, Germany, September 2012.

[33] Arienti, M., Pan, W., Li, X., and Karniadakis, G., Journal of Chemical Physics 134: 204114 (2011).